Published by
NIGERIAN SOCIETY OF PHYSICAL SCIENCES
Available online @ https://journal.nsps.org.ng/index.php/jnsps

J. Nig. Soc. Phys. Sci. 7 (2025) 2917

Journal of the Nigerian Society of Physical Sciences

Zinc oxide nanoparticles and nanorods: advanced sunscreen ingredients for enhanced UV protection and radiation filtration

Ammar A. Oglat[a,*], Abdallah Al Said[b], Naser M. Ahmed[c], Mohammed Dawood Salman[d]

[a]*Department of Medical Imaging, Faculty of Applied Medical Sciences, The Hashemite University, Zarqa,13133, Jordan*
[b]*School of Physics, Universiti Sains Malaysia, 11800 USM Penang, Malaysia*
[c]*Laser and Optoelectronics Engineering Department, Dijlah University College, Baghdad, Iraq*
[d]*Department of Medical Physics, College of Applied Sciences, University of Fallujah, Iraq*

Abstract

Due to its high ability to absorb ultraviolet rays in a wide spectrum, zinc oxide has emerged as the most important element used in the manufacture of sunscreens and cosmetics. This study aimed to determine the composition of zinc oxide nanorods and nanoparticles, as well as their impact on UV ray absorption. This was done by using Field Emission Scanning Electron Microscopy (FESEM-EDS) and Ultra Violet (UV-Visible) spectroscopy to look at sunscreen samples that had different amounts of zinc oxide added to them. We prepared two types of commercial zinc oxide powder using a chemical bath deposition method. After characterizing samples of the two powders using FESEM-EDS spectroscopy, various shapes emerged, with rods dominating in both powders. The length of the structure was 224.7 nm, 9.443 μm, and the diameter was 75.65 nm, 859.9 nm, respectively. The sun protection factor and the critical wavelength for the prepared samples were calculated using UV-Visible spectroscopy to measure the absorbance. An increasing zinc oxide to a certain extent led to an increase in UV ray absorption in all regions of the UV ray wavelength, with the ideal zinc oxide ratio being. The sunscreen had a concentration of 27.5%, and the use of zinc oxide provided broad protection from ultraviolet rays in all samples at the critical wavelength. In conclusion, increasing zinc oxide concentration in sunscreen increased the sun protection factor, critical wavelength, and UV ray protection.

DOI:10.46481/jnsps.2025.2917

Keywords: Zinc oxide, UV absorption, Nanoparticles, Sunscreen, Sun protection factor (SPF), Critical wavelength

Article History :
Received: 08 May 2025
Received in revised form: 23 June 2025
Accepted for publication: 24 June 2025
Available online: 30 June 2025

Communicated by: B. J. Falaye

1. Introduction

Nanotechnology constitutes a comprehensive interdisciplinary field of inquiry. There has been progress and industrial engagement in the domain of nanotechnology [1–3]. The global economy has experienced remarkable growth during the past decade [4, 5]. It is a transdisciplinary assemblage of physical, chemical, biological, engineering, and electronic processes, materials, applications, and concepts, distinguished primarily by scale [6, 7]. It involves the manufacturing, manipulation, and application of materials within a defined size range. The range reaches a maximum of 100 nm [8, 9]. Nanotechnology may be regarded It includes four primary domains: nanomedicine, nanofabrication, nanometrology, and nanomaterials (NMs)/nanoparticles (NPs) [10, 11].

Engineered nanoparticles (ENPs) can improve sunscreens, paints, cosmetics, textiles, construction materials, electronics, and personal care products due to their unique physicochemical properties [12–15]. Nanotechnology improves the world econ-

*Corresponding author Tel. No.: +96-279-631-1835.
Email address: ammar.oglat@yahoo.com (Ammar A. Oglat)

omy but poses health dangers. NP production, transportation, and manipulation workers, as well as consumers and deliberate users of NPs for medicinal, imaging, and gene delivery, may be affected [16, 17].

Despite the lack of established human or occupational disorders linked to engineered nanomaterials (ENPs), we must address their risks [18, 19]. This constraint may be due to nanotoxicology's youth and the lack of technique for human epidemiological investigations of manufactured nanoparticle exposures. Given the weak association between particle mass and particle number, most ambient air monitoring focuses on particle mass, which may explain some human biomonitoring research on engineered nanoparticles (ENPs) and their health effects [20, 21].

In vitro methods are often used to estimate ENP exposure concerns due to biomonitoring data shortages. Most in vitro investigations use acute exposure and high doses [22, 23]. These acute toxicity studies may not be enough to extrapolate to actual exposure settings and assess engineered nanoparticle health risks [24–26]. Given this problem, realistic exposure conditions may involve in vitro long-term or chronic exposure to low or harmless levels. Few studies have shown the importance of low-dose in vitro chronic exposures to engineered nanoparticles (ENPs) [27].

UV light can create vitamin D3 or be used with drugs to cure psoriasis and vitiligo, but it can potentially cause skin cancer [28, 29]. Common malignancies include skin cancer. The global incidence of UV-induced melanoma and BCC/SCC is growing [30–32]. Sunshine is a continuous light spectrum with 45% UV, 5% visible, and 50% infrared [33, 34]. UV runs from 100 to 400 nm. Long wave UVA (315–400 nm), medium wave UVB (280–315 nm), and short wave UVC (100–280 nm) are the three wavelength classes recognised by the International Commission on Illumination [35]. The ozone layer efficiently absorbs UVC and 95% of UVB up to 310 nm. However, UVA is not absorbed. Ozone layer depletion increases UVB radiation worldwide. The majority of solar energy reaches humans as UVA. Long wave radiation darkens melanin 1000 times faster than UVB and penetrates deeper into the epidermis and dermis. UVA radiation too intense or long can burn weak skin and damage corium structures, prematurely aging it. Signs of early photoaging include wrinkles, wilting, laxity, sagging, uneven pigmentation, and dryness [36, 37]. The shape, size, and concentration of zinc oxide nanostructures significantly affect the UV absorption properties [37–40] and sun protection effectiveness of sunscreens. Zinc oxide nanorods and nanoparticles were found to enhance UV absorption across all UV wavelength regions. Specifically, increasing the concentration of zinc oxide in sunscreen up to an optimal level (27.5%) resulted in higher sun protection factor (SPF), increased critical wavelength, and broader UV protection. The structural characteristics—such as the rod-like morphology and nanoscale dimensions—contributed to this improved performance [41, 42].

Sunscreens prevent sunburn, but users may spend longer time in the sun because they feel protected. This scenario raises extra concerns. Because most sunscreens are UVB (290-320 nm), they sometimes contain short-wavelength UVAII (320-340 nm) filters and change the UVR spectrum. Long-wavelength UVR, 340 nm and higher, will increase if sunscreen usage changes behavior and prolongs sun exposure. Sunscreens prevent sunburn, but the threshold or dose-response for UVR-induced effects on immunosuppression or DNA damage is unknown. Finally, as sunscreens grow more popular and economical, questions about their long-term safety, especially in UVR, have arisen [43, 44].

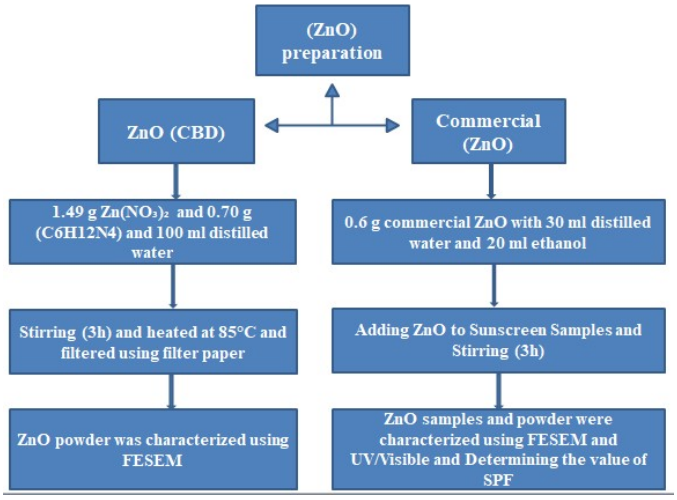

Figure 1: Steps and procedures used in the methodology section.

Zinc oxide has good chemical stability, electrochemical coupling coefficient, radiation absorption spectrum, and photostability [45–48]. Zinc oxide is a semiconductor in groups II-VI with a covalence between ionic and covalent. Its wide power range (3.37 eV), high bond energy (60 mV), and thermal/mechanical stability at ambient temperature make it suitable for use in electronics, optoelectronics, and laser technology [41, 42, 49]. Wurtzite zinc oxide is hexagonal (space group C6mc) with lattice parameters a = 0.3296 and c = 0.52065 nm. The basic structure of ZnO is alternating planes of tetrahedrally linked O2 and Zn2+ ions along the c-axis [49–52].

The aim of this study is to create a sunscreen that incorporates zinc oxide nanoparticles and nanorods, assess the sun protection factor (SPF) and critical wavelength of all samples, and ascertain the degree to which the zinc oxide addition influences these parameters.

2. Methodology

The method describes the preparation of a zinc oxide and sunscreen mixture using distilled water and ethanol, and outlines the procedures for characterizing the samples using FE-SEM and UV-Vis techniques. See Figure 1.

2.1. Samples preparation

In this research study, commercial zinc oxide powder (Sigma Aldrich) was used, and zinc oxide was also made

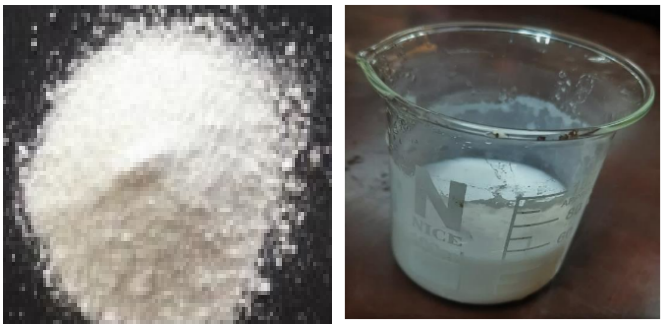

Figure 2: A solution of zinc oxide with distilled water and ethanol.

by the synthesized chemical bath deposition (CBD) method [53, 54], where zinc nitrite $(NO_3)_2$ and hexamine $(C_6H_{12}N_4)$ were used in certain proportions for its manufacture. The samples were prepared by mixing commercial zinc with distilled water, ethanol, and sunscreen. After weighing 0.6 g of commercial zinc oxide powder with an electronic weighing machine, we transferred it to a glass beaker, added 30 ml of distilled water and 20 ml of ethanol, mixed the solution for an hour with a magnetic stirrer, and then used an ultrasonic tank for 30 minutes to separate the suspended particles and remove impurities. The maximum solubility of zinc oxide powder is observed in a 40% ethanol and 60% distilled water solution. Figure 2 illustrates the preparation of zinc oxide solution using commercial zinc oxide powder, distilled water, and ethanol.

After making zinc oxide solution, 4 sunscreen samples were made with ethanol and distilled water. The sunscreen was most soluble in 60:40 distilled water and ethanol. All sample preparation will be explained in order. After preparing a 60:40 solutions of distilled water and ethanol in the first sample, 1 ml of sunscreen was transferred to a glass beaker using a fine syringe, 9 ml of the previously prepared solution was added, and 1 ml of the previously prepared ZnO solution was added. This sample was labeled. The second sample, labeled (2ml), included 1 ml of sunscreen, 8 ml of distilled water and ethanol, and 2 ml of ZnO solution. The third sample, labeled 3ml, included 1 ml of sunscreen, 7 ml of distilled water and ethanol, and 3 ml of ZnO. In the final sample, 1 ml of sunscreen was placed to a glass beaker with 6 ml of distilled water and ethanol and 4 ml of ZnO.

The Ultrasonic Tank cleaned and purified this study's instruments before preparing samples. Using a magnetic hotplate stirrer and magnetic stirrer bar, the samples were mixed for 3 hours to melt the sunscreen in all samples, which contained On 11 ml of the mixture in various amounts as described. After preparing all the samples, it was noticed that their high density was diminished, so 1 ml of each sample was transferred to a glass beaker and 8 ml of 60:40 distilled water and ethanol solution was added, resulting in four diluted samples with the same names. The samples were mixed again with a magnetic hotplate stirrer and magnetic stirrer bar for 1 hour to mix the solution components. The Ultrasonic Tank also separated solution particles and removed contaminants from all samples using high-frequency sound waves. See Figure 3.

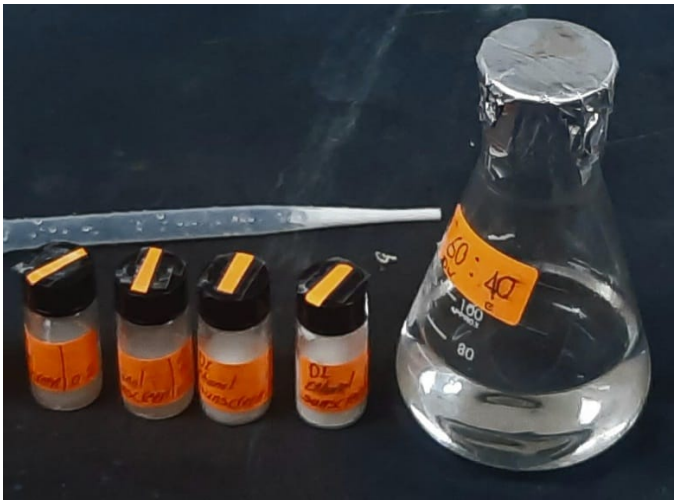

Figure 3: The prepared samples along with the pre-made distilled water and ethanol solution.

Figure 4: Materials and tools are used in the manufacture of zinc oxide powder by chemical bath deposition (CBD) such as $Zn(NO_3)_2$ and $(C_6H_{12}N_4)$.

2.2. *Zinc oxide manufacture using Chemical bath deposition (CBD) method*

In order to prepare zinc oxide powder using the CBD method, 1.49 g of zinc nitrate powder and 0.70 g of hexamine powder were added to a glass beaker, weighed them using an electronic weighing machine, added 100 ml of distilled water, and used a magnetic stirrer to mix the materials for 3 hours. Next, an ultrasonic tank was used for 30 minutes to separate the solid particles from the liquid particles in the solution and remove the impurities using the high-frequency sound waves generated by the device. Finally, the solution was placed in a water bath at a temperature of 85°C for 5 hours. After the zinc oxide particles settle to the bottom, we use filter paper to separate them from the water molecules. The filter paper is placed in the funnel, the funnel is placed in a glass beaker, the solution is slowly passed from inside the funnel to filter out the zinc oxide particles, and then the filter paper is heated with a filter oven to get all the zinc oxide powder particles. See figure 4.

In this study, the molar equations were used to calculate the amount of hexamine and zinc nitrite required to prepare zinc oxide, with M for both elements set at 50 mM and a solution volume of 100 ml. It turns out that the amount of zinc needed

Table 1: Values of EE (λ) × I at a different wavelength [56].

Wavelength	Value of EE × I
290	0.0150
295	0.0817
300	0.2874
305	0.3278
310	0.1864
315	0.0837
320	0.0180

to prepare the sample is 1.49 g, and the amount of hexamine is 0.70 g, in addition to 100 ml of distilled water. The following are the equations used to calculate the amount of zinc and hexamine used in the manufacture of zinc oxide by the CBD method:

$$M = \frac{n}{v}, \tag{1}$$

$$n = \frac{m}{Mr}, \tag{2}$$

where M is the molarity of ZnO solution, n is the number of moles ZnO must be used, v is the volume of ZnO solution desired in liter, m is mass of ZnO nanopowder required and Mr is the relative molecular mass of ZnO.

3. Determination the values of Sun protection factor (SPF)

The SPF is a quantitative measurement of the effectiveness of a sunscreen formulation. To be effective in preventing sunburn and other skin damage, a sunscreen product should have a wide range of absorbance between 290 and 400 nm. The in vitro SPF is useful for screening tests during product development. This study employed a single sunscreen product, fixed the sunscreen percentage in four samples, and added zinc oxide in varying amounts to these samples. UV spectrophotometry evaluated the sunscreen samples using the Al-Mansour mathematical equation [55].

$$SPF = CF \times [EE(\lambda) \times I(\lambda) \times Abs(\lambda)], \tag{3}$$

where EE (λ) is erythemal effect spectrum, I (λ) is solar intensity spectrum; Abs (λ) is absorbance of sunscreen product, CF is correction factor (= 10).

Table 1 shows the absorbance values of the samples and the SPF values after calculating them using the Al-Mansour mathematical equation.

4. Critical wavelength (CW)

The critical wavelength (CW) of the samples characterized was studied using the ultraviolet-visible device to obtain the best benefit from the sunscreen. Each sample contained a fixed concentration of sunscreen and a different concentration of zinc oxide.

Using the critical wavelength (CW) of samples, particularly in UV-Vis spectroscopy and related analytical methods, offers several important benefits, especially when evaluating materials like sunscreens, polymers, or coatings. Critical wavelength is commonly used in sunscreen testing to quantify broad-spectrum UV protection. A product is considered "broad-spectrum" if its CW is ≥ 370 nm (based on FDA and ISO standards). This ensures protection not just against UVB (280–315 nm), which causes sunburn, but also UVA (315–400 nm), which contributes to aging and skin cancer.

The FDA has approved CW after evaluating the cost and effort of UVA or broad-spectrum sunscreen [57].

$$\int_{290}^{\lambda} A\lambda d\lambda = 0.9 \int_{290}^{400} A\lambda \, d\lambda. \tag{4}$$

Equation (4) was applied to the absorption values obtained from UV spectroscopy, and the CW value was determined for each sample. The Origin 2018 program was used to estimate the integrals and calculate the CW values.

5. Results and discussion

This section will explain how FESEM/EDS examined the morphology of commercial ZnO and ZnO powder made using the CBD method.

5.1. Structural analysis of commercial ZnO

Figure 5(a) depicts the Energy-dispersive X-ray spectroscopy (EDS) at 10 keV to determine the relative atomic ratio of ZnO powder. Various forms of ZnO powder, such as rods, grains, and sheets, were found in the rod structures that were prevalent, and the diameter and length were measured, as the diameter was 75.65 nm and the structure length was 224.7 nm, according to the FESEM micrographs in Figure 5(b). The hexagonal shape of the ZnO structures in Figure 5(b) also showed that the ZnO powder was crystalline wurtzite. FESEM-EDS Figure 5(a), which determined the proportion of ZnO powder composition, suggests a greater degree of ZnO purity. The visible peaks identify the Zn atom at 1 keV, 8.62 keV, and 9.58 keV, respectively, and the O atom at 0.51 keV. Moreover, in terms of atomic percentages and weight, the O: Zn ratio was 0.896 and 0.22, respectively. This result indicates that the oxygen atom content in this powder is lower than the zinc atom content, which is most likely due to defect development during the zinc oxidation process. Excess zinc can be ascribed to crystalline ZnO inherent defects such as oxygen vacancies and zinc interfacial materials [58].

The Energy-dispersive X-ray spectroscopy (EDS) at 10 keV revealed the relative atomic ratio of elements in the ZnO powder. The Field Emission Scanning Electron Microscopy (FESEM) micrographs showed that the ZnO powder exists in various morphological forms, including rods, grains, and sheets, with rod-like structures being the most prevalent. These rod structures had an average diameter of 75.65 nm and a length of 224.7 nm.

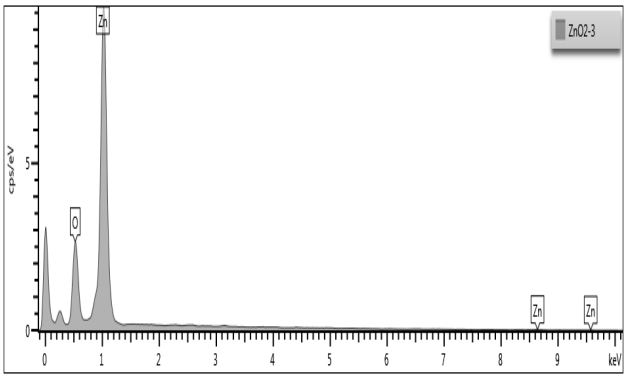

(a) Field Emission Scanning Electron Microscopy with Energy Dispersive X-ray Spectroscopy (FESEM-EDS) analysis of commercial zinc oxide, showing elemental composition.

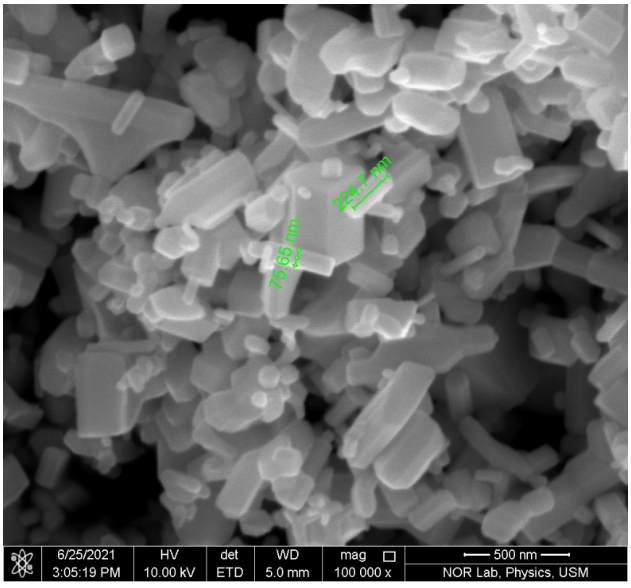

(b) FESEM micrograph depicting the surface morphology of commercial zinc oxide.

Figure 5: (a) FESEM-EDS analysis of commercial zinc oxide. (b) FESEM micrograph of commercial zinc oxide.

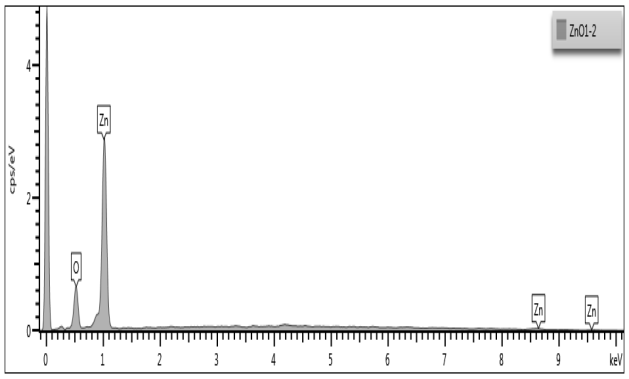

(a) FESEM-EDS analysis of zinc oxide synthesized via the chemical bath method, highlighting elemental composition.

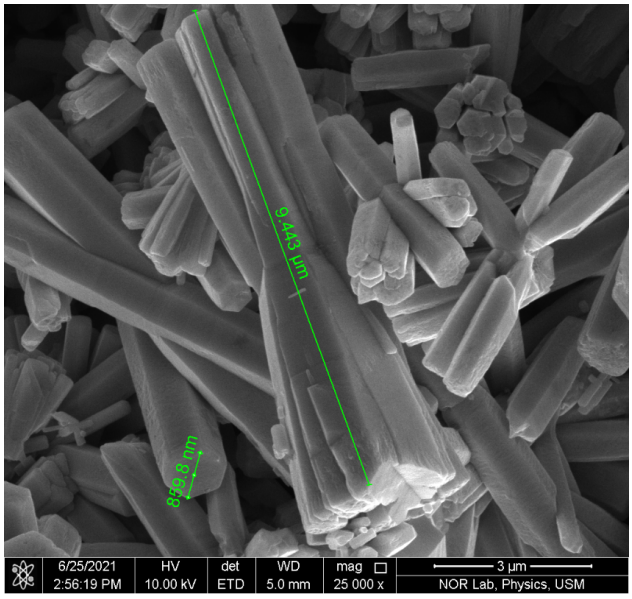

(b) FESEM micrograph showing the surface morphology of zinc oxide produced by the chemical bath method.

Figure 6: (A) FESEM-EDS analysis of synthesized zinc oxide. (B) FESEM micrograph of synthesized zinc oxide.

Figure 6(a) displays EDS at 10 keV that was used to figure out the relative atomic ratio of ZnO powder made by the chemical bath method. Figure 6 (B) shows FESEM images of ZnO powder. Most of the shapes were rod-shaped, and their structures were much bigger than rods in commercial zinc oxide. The structures had a diameter of 859.8 nm and a length of 9.443 μm. The FESEM-EDS analysis presents the percentage of ZnO powder composition in Figure 6(a), indicating a higher level of ZnO purity. The visible peaks indicate the Zn atom at 1 keV, 8.65 keV, and 9.59 keV, and the O atom at 0.50 keV, respectively. Moreover, the ratio of O: Zn in the measurement of atomic percentages and weight was 0.70 and 0.17, respectively.

This result indicates that the oxygen atom content in this powder is lower than that of zinc, likely due to the formation of defects during the zinc oxidation process, as observed in commercial zinc oxide. Furthermore, the UV performance can also be influenced by the particle size of ZnO nanorods. Particles smaller than 100 nm can effectively attenuate UV rays, thereby enhancing skin transparency and enhancing cosmetic values. ZnO nanorods have particle sizes between 61-70 nm, which are smaller than the UV wavelength, allowing them to absorb both UVB and UVA rays [59, 60].

5.2. *Optical absorption analysis*

A UV-visible device checked which samples of commercial zinc oxide dissolved in distilled water and ethanol at a 60:40 ratios were the best at blocking ultraviolet rays, especially those with a wavelength of 300 nm or more as shown in Figure 7.

Interpretation of the spectra is done by high absorbance at characteristic ZnO wavelengths (e.g., ~360–380 nm) suggests ZnO is well-dispersed in the solvent. Moreover, low or no absorbance may indicate poor dispersion or no dissolved parti-

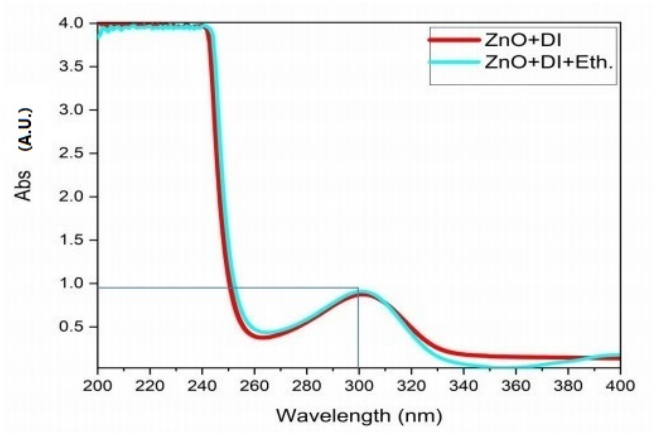

Figure 7: UV-Vis absorption spectrum of zinc oxide measured in two solvents: distilled water and a 60:40 (v/v) mixture of distilled water and ethanol.

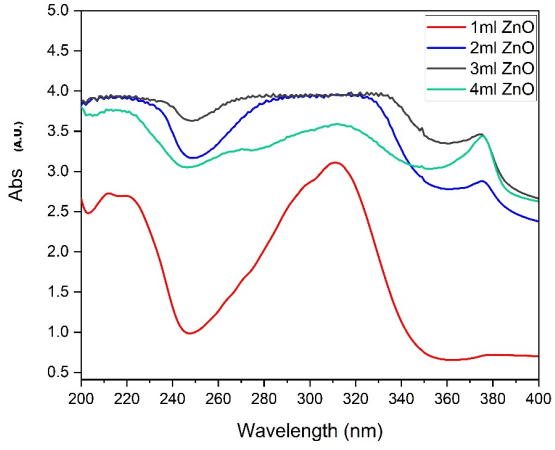

Figure 8: UV-Vis absorbance spectra of zinc oxide samples at varying concentrations.

cles. However, the broad peak or scattering baseline can indicate nanoparticle aggregation or turbidity.

Figure 8 shows that the absorption spectra of the sunscreen contain different concentrations of ZnO. After characterizing the sunscreen samples with different percentages of zinc oxide added using the UV-Visible device, we observed that zinc oxide significantly enhanced the sunscreen's protection against ultraviolet radiation across all wavelengths of ultraviolet rays by increasing its absorbance [61].

The first sample, which contained 1 ml of zinc oxide, exhibited the least absorption of ultraviolet rays. However, increasing the percentage of zinc oxide in the second sample to 2 ml significantly increased this absorption. The absorption of sunscreen significantly increased in the third sample, reaching its peak absorption of ultraviolet rays after increasing the zinc oxide proportion to 3 ml. However, the absorption of sunscreen decreased in the fourth sample after increasing the zinc oxide to 4 ml. Increasing the volume ratio of ZnO by 1 mL, 2 mL, and

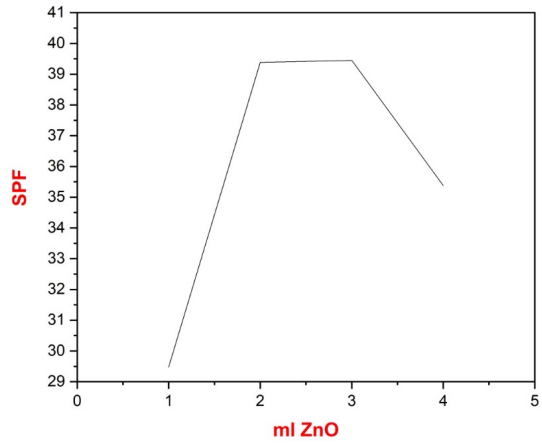

Figure 9: Variation in SPF values of sunscreen samples as a function of zinc oxide concentration.

3 mL in sunscreen increased the UV absorption as indicated by the red, blue, and black curves [62, 63].

By contrast, increasing the volume ratio of ZnO to 4 ml decreased the absorbance as shown by the green curve in Figure 8. The unique properties of ZnO NPs or a poorly dissolved mixture in the sample could be the cause of the sunscreen's reduced UV absorption when the volume of zinc oxide increases to 4 ml. Alternatively, an increase in UV reflection caused the absorption to decrease when the zinc oxide reached 4 ml. After increasing the zinc oxide proportion, we observed an increase in absorption in most UV wavelength regions, with the UVB and UVC regions experiencing the best effect, and the UVA region showing the least effect. We used it to absorb ultraviolet rays in all regions of the UV wavelength, noting that the average absorbance ranged from 3 to 4, indicating a good absorption of UV rays in all areas.

5.3. Sun protection factor (SPF)

The dilute UV method was employed to evaluate the SPF values of samples with volumes of 1 mL, 2 mL, 3 mL, and 4 mL. These samples had been previously diluted using a 60:40 mixtures of distilled water and ethanol. UV absorbance readings were recorded across the 290–320 nm range, at 5 nm intervals, using a UV-Vis spectrophotometer (Table 2). The Al-Mansour equation was then applied to calculate the SPF values. The absorbance values of the various formulas were found between 290 and 320 nm, and these values were multiplied by the corresponding EE (λ) values. Their sum was multiplied by the correction factor.

Table 3 summarizes the SPF values for sunscreen containing different concentrations of ZnO NPs and Sunscreen SPF30. The sample containing 1 ml of ZnO had the lowest SPF value at 29.47868, the second sample had an SPF value of 39.38863, and the third sample, which contained 3 ml of ZnO NPs, had a peak SPF value of 39.44397. A decrease in the value of SPF was also observed in the fourth sample after the increase of

Table 2: SPF value and absorbance for samples (1ml, 2ml, 3ml and 4ml).

Sample Name	1 ml		2 ml		3 ml		4 ml	
Wavelength (nm)	Abs	SPF	Abs	SPF	Abs	SPF	Abs	SPF
290	2.53583	0.380375	3.91218	0.586827	3.929706	0.589456	3.432081	0.514812
295	2.724328	2.225775	3.922783	3.204913	3.932561	3.212902	3.470883	2.83571
300	2.865462	8.235338	3.922177	11.27234	3.957174	11.37292	3.513244	10.09706
305	2.986163	9.78864	3.947452	12.93974	3.927089	12.87297	3.546132	11.62422
310	3.1052	5.788	3.952774	7.3679	3.956493	7.3749	3.581647	6.67619
315	3.05232	2.55479	3.951164	3.307124	3.95369	3.30923	3.577255	2.99416
320	2.809791	0.505762	3.943313	0.70979	3.95329	0.711592	3.522748	0.634095
SPF value	1ml ZnO	29.47868	2ml ZnO	39.38863	3ml ZnO	39.44397	4ml ZnO	35.37625

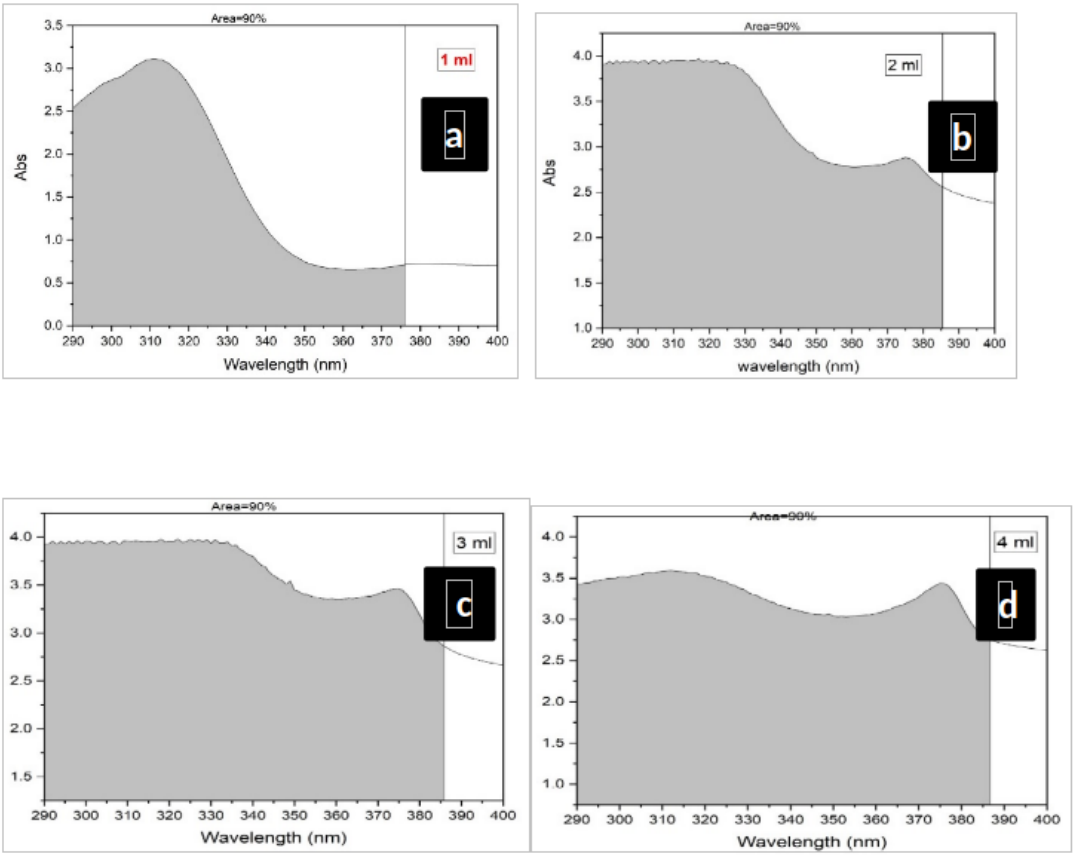

Figure 10: Critical wavelength values of sunscreen samples containing zinc oxide.

Table 3: Sun protection factor values of different formulations.

Samples	Sun Protection Factor (SPF)
1ml ZnO	29.47868
2ml ZnO	39.38863
3ml ZnO	39.44397
4ml ZnO	35.37625

Table 4: The Critical wavelength values of all samples.

Samples	Critical wavelength (nm)
1ml	376
2ml	385.5
3ml	386
4ml	387

ZnO NPs to 4 ml, where the SPF value in the fourth sample was 35.37625.

5.4. Critical wavelength (CW)

Table 4 and Figure 10 revealed that all samples had a CW greater than 370 nm and demonstrated good UVA protection. It was also observed that the increase in the concentration of zinc

oxide in the sunscreen increases CW.

In the first sample, in the Figure 10(a), 1 ml ZnO was added. The critical wavelength was 376 nm. With an increase in the concentration of ZnO in the second sample to 2 ml (Figure 10(b)), the CW value increased to 385.5 nm. In the third sample (Figure 10(c)), it became The CW value was 386 nm after increasing the concentration of ZnO to 3 ml, and in the fourth sample (Figure 10(d)), which had the highest concentration of zinc oxide, 4 ml, the CW value was 387 nm, which reached the highest UVA protection.

6. Conclusion

Increasing the concentration of zinc oxide in sunscreen formulations significantly improves their effectiveness in shielding the skin from harmful ultraviolet (UV) radiation. As the amount of zinc oxide rises, the sunscreen's capacity to absorb and scatter UV rays is enhanced, leading to a higher Sun Protection Factor (SPF) and more comprehensive coverage across both UVA and UVB wavelengths. Through testing and analysis, a concentration of 27.5% zinc oxide has been identified as optimal. At this level, the sunscreen provides robust protection, particularly at the critical wavelength—an important benchmark for evaluating the depth and breadth of UVA defense.

Data availability

All data generated or analysed during this study are included in this published.

References

[1] B. Bhushan, *Introduction to nanotechnology*, Springer, Berlin, Heidelberg, 2017, pp. 1–19. https://doi.org/10.1007/978-3-662-54357-3_1.

[2] E. Y. Salih, A. Ramizy, O. Aldaghri, M. H. Eisa & K. H. J. M. L. Ibnaouf, "Solution processed self-powered broadband flower-like Zn (Al) O-mixed metal oxide dye sensitized photodetector", Materials Letters **362** (2024) 136213. https://doi.org/10.1016/j.matlet.2024.136213.

[3] A. H. Rajpar, M. B. A. Bashir, E. Y. Salih & E. M. J. N. Ahmed, "Fabrication and enhanced performance evaluation of TiO2@ Zn/Al-LDH for DSSC application: The influence of post-processing temperature", Nanomaterials **14** (2024) 920. https://doi.org/10.3390/nano14110920.

[4] M. C. Roco, "The long view of nanotechnology development: the National Nanotechnology Initiative at 10 years", Journal of Nanoparticle Research **13** (2024) 427. https://doi.org/10.1007/s11051-010-0192-z.

[5] M. Ali Dheyab, A. Abdul Aziz, M. S. Jameel, P. Moradi Khaniabadi & A. A. Oglat, "Rapid sonochemically-assisted synthesis of highly stable gold nanoparticles as computed tomography contrast agents", Applied Sciences **10** (2020) 7020. https://doi.org/10.3390/app10207020.

[6] W. S. Khan, E. Asmatulu & R. Asmatulu, "Nanotechnology emerging trends, markets and concerns", in *Nanotechnology safety*, Elsevier, 2025, pp. 1–21. http://dx.doi.org/10.1016/B978-0-444-59438-9.00001-1.

[7] S. Yeoh, M. Matjafri, K. Mutter & A. A. Oglat, "Plastic fiber evanescent sensor in measurement of turbidity", Sensors and Actuators A: Physical **285** (2019) 1. http://dx.doi.org/10.1016/j.sna.2018.10.042.

[8] M. Nasrollahzadeh, S. M. Sajadi, M. Sajjadi & Z. Issaabadi, "An introduction to nanotechnology", in *Interface science and technology*, Elsevier, 2019, pp. 1–27. https://doi.org/10.1016/B978-0-12-813586-0.00001-8.

[9] A. S. ALmomani, A. F. Omar, A. A. Oglat, S. S. Al-Mafarjy, M. A. Dheyab & T. H. J. S. Khazaalah, "Developed a unique technique for creating stable gold nanoparticles (AuNPs) to explore their potential against cancer", South African Journal of Chemical Engineering **53** (2025) 142. https://doi.org/10.1016/j.sajce.2025.04.012.

[10] S. Mohapatra, S. Ranjan, N. Dasgupta, S. Thomas & R. K. Mishra, "Characterization and Biology of nanomaterials for drug delivery: nanoscience and nanotechnology in drug delivery", in *Nanoscience and nanotechnology in drug delivery*, Elsevier, 2018, pp. 1–27. https://doi.org/10.1016/B978-0-12-813586-0.00001-8.

[11] E. Y. Salih, M. F. M. Sabri, M. Z. Hussein, K. Sulaiman, S. M. Said, B. Saifullah & M. B. Bashir, "Structural, optical and electrical properties of ZnO/ZnAl 2 O 4 nanocomposites prepared via thermal reduction approach", Journal of Materials Science **53** (2018) 581. https://link.springer.com/article/10.1007%2Fs10853-017-1504-9.

[12] N. Prajitha, S. Athira & P. J. Mohanan, "Bio-interactions and risks of engineered nanoparticles", Environmental Research **172** (2019) 98. https://doi.org/10.1016/j.envres.2019.02.003.

[13] Q. Abbas, B. Yousaf, M. U. Ali, M. A. Munir, A. El-Naggar, J. Rinklebe & M. J. E. i. Naushad, "Transformation pathways and fate of engineered nanoparticles (ENPs) in distinct interactive environmental compartments: A review", Environment International **138** (2020) 105646. https://doi.org/10.1016/j.envint.2020.105646.

[14] M. A. Dheyab, P. M. Khaniabadi, A. A. Aziz, M. S. Jameel, B. Mehrdel, A. A. Oglat & H. A. J. P. Khaleel, "Focused role of nanoparticles against COVID-19: Diagnosis and treatment", Photodiagnosis and Photodynamic Therapy **34** (2021) 102287. https://doi.org/10.1016/j.pdpdt.2021.102287.

[15] O. F. Farhat, M. Husham, M. Bououdina, A. Abuelsamen, A. A. Oglat & N. J. Mohammed, "Tape-based novel ZnO nanoaggregates photodetector", Sensors and Actuators A: Physical **332** (2021) 113210. https://doi.org/10.1016/j.sna.2021.113210.

[16] M. A. Bhat, K. Gedik & E. O. Gaga, "Environmental impacts of nanoparticles: pros, cons, and future prospects", in *Synthesis of bionanomaterials for biomedical applications*, Elsevier, 2023, pp. 493–528. http://dx.doi.org/10.1016/B978-0-323-91195-5.00002-7.

[17] E. Y. Salih, Z. Abbas, S. H. H. Al Ali & M. Z. J. A. i. M. S. Hussein, "Dielectric behaviour of Zn/Al-NO3 LDHs filled with polyvinyl chloride composite at low microwave frequencies", Advances in Materials Science and Engineering **1** (2014) 647120. http://dx.doi.org/10.1155/2014/647120.

[18] B. Bocca, B. Battistini, V. Leso, L. Fontana, S. Caimi, M. Fedele & I. J. T. Iavicoli, "Occupational exposure to metal engineered nanoparticles: a human biomonitoring pilot study involving Italian nanomaterial workers", Toxics **11** (2023) 120. https://doi.org/10.3390/toxics11020120.

[19] G. Singh, N. Thakur & R. J. Kumar, "Nanoparticles in drinking water: Assessing health risks and regulatory challenges", Science of The Total Environment **1** (2024) 174940. https://doi.org/10.1016/j.scitotenv.2024.174940.

[20] C. Domingues, A. Santos, C. Alvarez-Lorenzo, A. Concheiro, I. Jarak, F. Veiga, I. Barbosa, M. Dourado & A. J. A. n. Figueiras, "Where is nano today and where is it headed? a review of nanomedicine and the dilemma of nanotoxicology", ACS Nano **16** (2022) 9994. https://doi.org/10.1021/acsnano.2c00128.

[21] A. Mohajerani, L. Burnett, J. V. Smith, H. Kurmus, J. Milas, A. Arulrajah, S. Horpibulsuk & A. J. M. Abdul Kadir, "Nanoparticles in construction materials and other applications, and implications of nanoparticle use", Materials **12** (2019) 3052. https://doi.org/10.3390/ma12193052.

[22] E. Bergamaschi, I. G. Canu, A. Prina-Mello & A. Magrini, "Biomonitoring", in *Adverse effects of engineered nanomaterials*, Academic Press, 2017, pp. 125–158. http://dx.doi.org/10.1016/B978-0-12-809199-9.00006-9.

[23] A. M. Lopes, H. U. Dahms, A. Converti & G. L. Mariottini, "Role of model organisms and nanocompounds in human health risk assessment", Environmental Monitoring and Assessment **193** (2021) 1. https://doi.org/10.1007/s10661-021-09066-2.

[24] D. Romeo, R. Hischier, B. Nowack, O. Jolliet, P. Fantke & P. J. Wick, "In vitro-based human toxicity effect factors: challenges and opportunities for nanomaterial impact assessment", Environmental Science: Nano **9** (2022) 1913. https://doi.org/10.1039/D1EN01014J.

[25] D. R. Hristozov, S. Gottardo, A. Critto & A. J. N. Marcomini, "Risk assessment of engineered nanomaterials: a review of available data and approaches from a regulatory perspective", Nanotoxicology **6** (2012) 880. https://doi.org/10.3109/17435390.2011.626534.

[26] B. Annangi, L. Rubio, M. Alaraby, J. Bach, R. Marcos & A. J. Hernández, "Acute and long-term in vitro effects of zinc oxide nanoparticles", Archives of Toxicology **90** (2016) 2201. https://doi.org/10.1007/s00204-015-1613-7.

[27] V. De Matteis, "Exposure to inorganic nanoparticles: routes of entry, immune response, biodistribution and in vitro/in vivo toxicity evaluation", Toxics **5** (2017) 29. https://doi.org/10.3390/toxics5040029.

[28] A. Juzeniene & J. Moan, "Beneficial effects of UV radiation other than via vitamin D production", Dermato-Endocrinology **4** (2012) 109. https://doi.org/10.4161/derm.20013.

[29] B. Wadhwa, V. Relhan, K. Goel, A. M. Kochhar & V. K. Garg, "Vitamin D and skin diseases: a review", Indian Journal of Dermatology, Venereology and Leprology **81** (2015) 344. https://doi.org/10.4103/0378-6323.159929.

[30] H. Soehnge, A. Ouhtit & O. Ananthaswamy, "Mechanisms of induction of skin cancer by UV radiation", Frontiers in Bioscience **2** (1997) 538. https://doi.org/10.2741/a211.

[31] B. Kozma & M. J. Eide, "Photocarcinogenesis: an epidemiologic perspective on ultraviolet light and skin cancer", Dermatologic Clinics **32** (2014) 301. https://doi.org/10.1016/j.det.2014.03.004.

[32] N. Hasan, A. Nadaf, M. Imran, U. Jiba, A. Sheikh, W. H. Almalki, S. S. Almujri, Y. H. Mohammed, P. Kesharwani & F. J. Ahmad, "Skin cancer: understanding the journey of transformation from conventional to advanced treatment approaches", Molecular Cancer **22** (2023) 168. https://doi.org/10.1186/s12943-023-01854-3.

[33] Y. Shi, J. Du & J. J. Qiu, "A novel double 3D continuous phase composite with ultra-broadband wave absorption from gigahertz to UV–vis-NIR for extremely cold environment", Chemical Engineering Journal **436** (2022) 135220. https://dx.doi.org/10.2139/ssrn.3994402.

[34] J. Li, N. Arif, T. Lv, H. Fang, X. Hu & Y. Zeng, "Towards full-spectrum photocatalysis: Extending to the near-infrared region", ChemCatChem **14** (2022) e202200361. https://doi.org/10.1002/cctc.202200361.

[35] S. B. Saha, A. Saha, P. Das, A. Kakati, A. Banerjee & P. Chattopadhyay, "A comprehensive review of ultraviolet radiation and functionally modified textile fabric with special emphasis on UV protection", Heliyon **10** (2024) e40027. https://doi.org/10.1016/j.heliyon.2024.e40027.

[36] A. Svobodova, D. Walterova & J. Vostalova, "Ultraviolet light induced alteration to the skin", Biomedical Papers-Palacky University in Olomouc **150** (2006) 25. https://doi.org/10.5507/bp.2006.003.

[37] M. D. Salman, Y. M. Radzi, E. Y. Salih, A. A. Oglat, A. A. Rahman & M. A. Dheyab, "Synthesis techniques and modern applications of copper oxide nanoparticles in cancer treatment and radiotherapy: A review", Journal of Molecular Structure **1322** (2024) 140301. http://dx.doi.org/10.1016/j.molstruc.2024.140301.

[38] M. D. Salman, Y. M. Radzi, A. A. Oglat, R. W. Kolaib, A. Idris, M. Alhassan, W. A. Alton & A. Rahman, "Enhancing the acoustic properties for a novel radiation dosimetry PMMAG by optimizing the stability of copper oxide nanoparticles", BioNanoScience **15** (2025) 1. http://dx.doi.org/10.1007/s12668-025-01900-y.

[39] M. D. Salman, Y. M. Radzi, A. A. Rahman & A. A. Oglat, "Ultrasound evaluation of polymathic methacrylate (PMMA) gel dosimeter doped with copper oxide (CuO) nanoparticles", Physica Scripta **99** (2024) 085307. http://dx.doi.org/10.1088/1402-4896/ad623b.

[40] A. Abuelsamen, S. Mahmud, G. N. Makhadmeh, T. AlZoubi, A. Al Diabat, N. A. Algadri, O. A. Noqta, E. Absi, A. M. S. A. Majid & A. A. Oglat, "Pluronic F-127-coated ZnO nanoparticles as superior photosensitizers for effective bladder cancer photodynamic therapy: In-vitro evaluation", Journal of Drug Delivery Science and Technology **95** (2024) 105550. http://dx.doi.org/10.1016/j.jddst.2024.105550.

[41] O. Farhat, M. Halim, N. M. Ahmed, A. A. Oglat, A. Abuelsamen, M. Bououdina & M. J. Qaeed, "A study of the effects of aligned vertically growth time on ZnO nanorods deposited for the first time on Teflon substrate", Applied Surface Science **426** (2017) 906. https://doi.org/10.1016/j.apsusc.2017.07.031.

[42] U. Bashir, Z. Hassan, N. M. Ahmed, A. Oglat & A. J. Yusof, "Sputtered growth of high mobility InN thin films on different substrates using Cu-ZnO buffer layer", Materials Science in Semiconductor Processing **71** (2017) 166. https://doi.org/10.1016/j.mssp.2017.07.025.

[43] J. K. Robinson, S. Patel, S. Y. Heo, E. Gray, J. Lim, K. Kwon, Z. Christiansen, J. Model, J. Trueb & A. Banks, "Real-time UV measurement with a sun protection system for warning young adults about sunburn: prospective cohort study", JMIR mHealth and uHealth **9** (2021) e25895. https://doi.org/10.2196/25895.

[44] O. P. Egambaram, S. Kesavan Pillai & S. Ray, "Materials science challenges in skin UV protection: a review", Photochemistry and Photobiology **96** (2020) 779. https://doi.org/10.1111/php.13208.

[45] H. Gulab, N. Fatima, U. Tariq, O. Gohar, M. Irshad, M. Z. Khan, M. Saleem, A. Ghaffar, M. Hussain & A. Jan, "Advancements in zinc oxide nanomaterials: synthesis, properties, and diverse applications", Nano-Structures & Nano-Objects **39** (2024) 101271. https://doi.org/10.1016/j.nanoso.2024.101271.

[46] A. A. Oglat, "Gamma ray, beta and alpha particles as a sources and detection", Journal of Radiation Research and Applied Sciences **16** (2023) 100503. https://doi.org/10.1016/j.jrras.2022.100503.

[47] A. A. Oglat, "Comparison of X-ray films in term of kVp, mA, exposure time and distance using Radiographic Chest Phantom as a radiation quality", Journal of Radiation Research and Applied Sciences **15** (2022) 100479. http://dx.doi.org/10.1016/j.jrras.2022.100479.

[48] R. Abdalrheem, F. Yam, A. R. Ibrahim, H. Lim, K. Beh, O. F. Farhat, A. A. Oglat & A. Abuelsamen, "Exploring 1-butanol as a potential liquid precursor for graphene synthesis via chemical vapour deposition and enhanced catalyzed growth methodology", Journal of Nanoparticle Research **21** (2019) 1. https://doi.org/10.1007/s11051-019-4650-y.

[49] O. F. Farhat, M. Hisham, M. Bououdina, A. A. Oglat & N. Mohammed, "Growth of ZnO nanostructures by wet oxidation of Zn thin film deposited on heat-resistant flexible substrates at low temperature", Semiconductors **54** (2020) 1220. http://dx.doi.org/10.1134/S1063782620100103.

[50] O. V. Yakubovich, G. V. Kiriukhina, A. S. Volkov & O. V. Dimitrova, "A rare case of Na/Zn isomorphism in the crystal structure of acentric zincophosphate Na5Zn [Zn (PO4) 3]", Structural Science **81** (2025) 62. https://doi.org/10.1107/s2052520624011156.

[51] X. Zhao, C. Yang & M. J. Chen, "Aqueous multivalent metal ion batteries: Fundamental mechanism and applications", in *Towards next generation energy storage technologies: From fundamentals to commercial applications*, 2024, pp. 249–287. http://dx.doi.org/10.1002/9783527845316.ch7.

[52] M. Alshipli, T. A. Altaim, M. Aladailah, A. A. Oglat, S. A. Alsenany, O. Tashlykov, S. M. F. Abdelaliem, M. Marashdeh, R. Banat & D. J. Pyltsova, "High-density polyethylene with ZnO and TiO2 nanoparticle filler: Computational and experimental studies of radiation-protective characteristics of polymers", Journal of Radiation Research and Applied Sciences **16** (2023) 100720. https://doi.org/10.1016/j.jrras.2023.100720.

[53] R. Abdalrheem, F. Yam, A. R. Ibrahim, H. Lim, K. Beh, A. A. Ahmed, A. A. Oglat, K. M. Chahrour, O. F. Farhat & N. J. Afzal, "Improvement in photodetection characteristics of graphene/p-Silicon heterojunction photodetector by PMMA/graphene cladding layer", Journal of Electronic Materials **48** (2019) 4064. http://dx.doi.org/10.1007/s11664-019-07170-1.

[54] R. Abdalrheem, F. Yam, A. R. Ibrahim, K. Beh, Y. Ng, F. Suhaimi, H. Lim, M. M. Jafri & A. A. Oglat, "Comparative studies on the transfer of chemical vapor deposition grown graphene using either electrochemical delamination or chemical etching method", in *Journal of Physics: Conference Series*, IOP Publishing, 2018, p. 012038. http://dx.doi.org/10.1088/1742-6596/1083/1/012038.

[55] E. A. Dutra, D. A. Oliveira, E. Kedor-Hackmann & M. I. Santoro, "Determination of sun protection factor (SPF) of sunscreens by ultraviolet spectrophotometry", Revista Brasileira de Ciências Farmacêuticas **40** (2004) 381. http://dx.doi.org/10.1590/S1516-93322004000300014.

[56] E. Elahi, M. F. Khan, S. Rehman, H. W. Khalil, M. A. Rehman, D. Kim, H. Kim, K. Khan, M. Shahzad & M. W. Iqbal, "Enhanced electrical and broad spectral (UV-Vis-NIR) photodetection in a Gr/ReSe 2/Gr heterojunction", Dalton Transactions **49** (2020) 10017. http://dx.doi.org/10.1039/D0DT01164A.

[57] N. S. Bora, M. P. Pathak, S. Mandal, B. Mazumder, R. Policegoudra, P. S. Raju & P. Chattopadhyay, "Safety assessment and toxicological profiling of a novel combinational sunprotective dermal formulation containing melatonin and pumpkin seed oil", Regulatory Toxicology and Pharmacology **89** (2017) 1. https://doi.org/10.1016/j.yrtph.2017.07.004.

[58] A. Ali, A.-R. Phull & M. Zia, "Elemental zinc to zinc nanoparticles: Is ZnO NPs crucial for life? Synthesis, toxicological, and environmental concerns", Nanotechnology Reviews **7** (2018) 413. http://dx.doi.org/10.1515/ntrev-2018-0067.

[59] T. H. Kim, S. H. Park, S. Lee, A. S. Bharadwaj, Y. S. Lee, C. G. Yoo & T. H. Kim, "A review of biomass-derived UV-shielding materials for bio-composites", Energies **16** (2023) 2231. https://doi.org/10.3390/en16052231.

[60] A. A. Oglat, S. M. Shalbi & M. Suhimi, "Adding barium sulfate (BaSO4) to fly ash geopolymer increases its compressive strength as X-ray shielding for medical imaging applications", Cleaner Waste Systems **9** (2024) 100175. http://dx.doi.org/10.1016/j.clwas.2024.100175.

[61] M. Alshipli, M. Aladailah, M. Marashdeh, A. A. Oglat, H. Akhdar, O. Tashlykov, R. Banat & A. T. Walaa, "Fe-nanoparticle effect on polypropylene for effective radiation protection: Simulation and theoretical study", Medical Engineering & Physics **121** (2023) 104066. https://doi.org/10.1016/j.medengphy.2023.104066.

[62] E. T. Salim, M. A. Fakhri, S. M. Tariq, A. S. Azzahrani, R. K. Ibrahim, A. A. Alwahib, S. F. H. Alhasan, A. Ramizy, E. Y. Salih & Z. T. Salim, "The unclad single-mode fiber-optic sensor simulation for localized surface plasmon resonance sensing based on silver nanoparticles embedded coating", Plasmonics **19** (2024) 131. https://doi.org/10.1007/s11468-023-01949-z.

[63] M. K. Mohammed, A. M. Naji, D. S. Ahmed, M. J. Jamai, E. Y. Salih, M. Dehghanipour, S. Bhattarai, R. Pandey, J. Madan & M. F. Rahman, "Facile synthesis of chitosan-MoS2 over reduced graphene oxide to improve photocatalytic degradation of methylene blue", Journal of Sol-Gel Science and Technology **1** (2024) 1. https://doi.org/10.1007/s10971-024-06619-y.